Int. J. Mech. Sci. Vol. 25, No. 1, pp. 47–57, 1983
Printed in Great Britain.

0020/7403/83/010047–11$03.00/0
Pergamon Press Ltd.

NECKING IN UNIAXIAL TENSION

LI GUO CHEN†
Institute of Mechanics, Academia Sinica, Beijing, China

(*Received* 19 *April* 1981; *in revised form* 14 *May* 1982)

Summary—Applying two theories in plasticity (flow theory and a modified deformation theory), the necking of a cylindrical bar in uniaxial tension is analysed. The development of finite strain in the bar is handled by the up-dated Lagrangian description and the governing variational equation is solved by using a finite-difference discretization in the axial direction coupled with a polynomial representation of the radial fields. The accuracy of the solution is ensured through the use of Lagrange multipliers which enforce stress-free lateral boundary conditions. The computation proceeds by adjusting the plastic moduli of the material so that its force-displacement record agrees with that of an experiment. The comparison between the thinning of the neck predicted by the simulation and that measured experimentally provides a check on the constitutive assumptions used in the computation. Finally, the development of stress within the neck is presented.

NOTATION

τ^{ij} Kirchhoff stress tensor
σ^{ij} true stress tensor (also called Euler or Cauchy stress tensor)
T^{ij} nominal stress tensor (or Lagrange stress tensor)
V_i velocity of displacement vector, i.e. $V_i = \dot{U}_i$
D_{ij} strain rate tensor, $D_{ij} = (1/2)(V_{j|i} + V_{i|j})$
$\dot{F}^i$ load rate vector
g^{ij}, g_{ij} metric tensor
$\frac{\mathcal{D}}{\mathcal{D}_t}(\ )$ Jaumann derivative
$|_j$ covariant derivative
t generalized time
v volume
s boundary area (with known applied force)
n_j unit normal vector of the boundary area
$\dot{(\ )}$ convected derivative
E, ν Young's modulus and Poisson's ratio
r, θ, z cylindrical polar coordinates
R the maximum initial radius of the bar
L half length of the bar
r_0 the minimum current radius of the bar
U, W radial and axial displacements
D_e equivalent strain rate
σ_e equivalent stress
ϵ_e equivalent strain
σ_y yield stress

superscript (p) refers to plasticity.

INTRODUCTION

In order to analyse ductile fracture, one needs a proper description of the plastic response of the material under conditions of large strain. Once a particular theory has been chosen (e.g. von Mises flow theory or a deformation type of theory) the required constitutive response is uniquely specified by the result of a simple test, usually taken to be the uniaxial tensile test. Since the stress and strain within the neck are highly non-uniform the raw results of the test cannot be used directly to interpret ductile fracture and one has to resort to a computer simulation[1]. Such a simulation beyond the point of necking will provide information on the fields of stress and strain as they develop within the neck. This is very important to an attempt at modelling ductile fracture and may enable the analyst to formulate criterion for the onset of ductile fracture, when he compares his computations with experimental observations on the

†Name in Chinese phonetic spelling with surname first. Presently at Department of Mechanical Engineering, the University of Sheffield, Sheffield, England.

failure of the bar. These reasons, and others, have prompted research workers in the past to compute the necking of a bar. References [1–4] provide a résumé of previous work in this field.

Both Norris *et al.*[1] and Saje[3] solved two-dimensional problems using finite-difference methods. Chen[2], as here, used a compound method with an axial finite-difference representation coupled with a radial polynomial expansion, whilst Needleman[4] made use of a finite-element method. Both Chen and Norris *et al.* introduced an artificial taper into the bar in order to initiate necking, and Chen concluded that the results would differ only slightly if the size of the imperfection at the centre of the bar was small. Saje assumed the two ends of a perfect bar to be cemented to rigid grips. Needleman analysed a perfect bar with both shear-free ends and cemented ends. In the case of shear-free ends, he used a bifurcation criterion to start necking. The works of [2–4] were performed in Lagrangian coordinates, whilst Norris *et al.*[1] used a spatial description.

The present work uses the up-dated Lagrangian approach (for which Hill[5] and McMeeking and Rice[6] provide the basic variational equations). The representation of the field of velocity is similar to that of Chen, but with more terms in the radial expansion, an extension which calculations suggest is necessary in order to achieve the desired accuracy. Furthermore, in order to ensure a reasonable representation of the stress-free lateral sides, it is necessary to enforce that condition through the use of Lagrange multipliers. The simulation is for A-533 Grade B Class 1 nuclear pressure vessel steel, the experimental data being taken from Ref. [1].

Finally, the question of whether flow theory or deformation theory is a more appropriate representation of plastic flow (to which the recent development[7, 8] of corner theory may provide some answers) is addressed by performing the computations with both flow theory and a modified deformation theory.

VARIATIONAL EQUATIONS OF EQUILIBRIUM

According to Hill[5] and McMeeking and Rice[6], ensuring that the functional

$$I = \frac{1}{2}\int_v \left[\frac{\mathscr{D}\tau^{ij}}{\mathscr{D}t} D_{ij} - \sigma^{ij}(2D_{ik}D_{jl}g^{kl} - V^k{}_{|i}V_{k|j})\right] \mathrm{d}v - \int_s \dot{F}^i V_i \,\mathrm{d}s \tag{1}$$

takes an extremum is equivalent to satisfying the equilibrium equations

$$\left[\frac{\mathscr{D}\tau^{ij}}{\mathscr{D}t} - \sigma^{ik}D_k{}^j - \sigma^{jk}D_k{}^i + \sigma^{ik}V^j{}_{|k}\right]\Big|_i = \dot{T}^{ij}{}_{|i} = 0 \tag{2}$$

together with the boundary conditions

$$\left[\frac{\mathscr{D}\tau^{ij}}{\mathscr{D}t} - \sigma^{ik}D_k{}^j - \sigma^{jk}D_k{}^i + \sigma^{ik}V^j{}_{|k}\right] n_j = \dot{F}^i. \tag{3}$$

We shall see later that rapid computation requires a simple possible representation of the field of velocity, but this may result in some of the boundary conditions not being as accurately satisfied as one would wish. The remedy adopted in this work is to force the correct behaviour on those side conditions that would otherwise be inaccurately obeyed through the use of appropriate Lagrange multipliers. This may be expressed symbolically in the following way.

Suppose that we wish to impose k side constraints of the form

$$K^i(\alpha_j) = 0,\ i = 1 \ldots k,\ j = 1 \ldots q \tag{4}$$

and $k < q$ where K^i are functions of α_j, which are the nodal values of a discrete representation of the field of velocity. Then the functional

$$I_\lambda = I - \lambda_i K^i \tag{5}$$

is such that an extremum with respect to the velocity field and the Lagrange multipliers λ_i produces both the equations of equilibrium (2) with the boundary conditions (3) and the side conditions (4).

CONSTITUTIVE RELATIONS FOR FINITE STRAIN

The constitutive relations used in this work are derived from conventional infinitesimal-strain elastic–plastic relations, through the use of the following principles.

(a) Stress is taken to be true (or Cauchy) stress.

(b) The infinitesimal strain increment is taken to represent the strain rate.

(c) The increment of stress in the small strain case is interpreted as the Jaumann derivative of Kirchhoff stress. This eliminates any possibility of rigid body motion entering the constitutive relations.

(d) Stress, strain and their increments are written as mixed tensors, so that their relationship can retain the same form as in Cartesian coordinates.

The total strain rate can be decomposed into an elastic and a plastic part as

$$D_j^i = D_j^{i(e)} + D_j^{i(p)}. \tag{6}$$

For flow theory, the constitutive relations are

$$D_j^i = \frac{1}{E}\left[(1+\nu)\frac{\mathcal{D}\tau_j^i}{\mathcal{D}t} - \nu\delta_j^i\frac{\mathcal{D}\tau_k^k}{\mathcal{D}t}\right] + \alpha\frac{9}{4E_{te}^{(p)}}\frac{S_j^i S_k^l}{\sigma_e^2}\frac{\mathcal{D}\tau_l^k}{\mathcal{D}t} \tag{7}$$

whilst for a type of modified deformation theory,† they become

$$D_j^i = \frac{1}{E}\left[(1+\nu)\frac{\mathcal{D}\tau_j^i}{\mathcal{D}t} - \nu\delta_j^i\frac{\mathcal{D}\tau_k^k}{\mathcal{D}t}\right] +$$

$$\alpha\left[\left(\frac{3}{2E_{se}} - \frac{1+\nu}{E}\right)\left(\frac{\mathcal{D}\tau_j^i}{\mathcal{D}t} - \frac{1}{3}\delta_j^i\frac{\mathcal{D}\tau_k^k}{\mathcal{D}t}\right) + \frac{9}{4}\left(\frac{1}{E_{te}} - \frac{1}{E_{se}}\right)\frac{S_j^i S_k^l}{\sigma e^2}\frac{\mathcal{D}\tau_l^k}{\mathcal{D}t}\right] \tag{8}$$

where

$$S_j^i = \sigma_j^i - \frac{1}{3}\delta_j^i\sigma_k^k = \sigma_j^i - \frac{1}{3}\delta_j^i g_{kl}\sigma^{kl}$$

$$\sigma_e = \left(\frac{3}{2}S_j^i S_i^j\right)^{1/2} = \left(\frac{3}{2}g_{ik}g_{jl}S^{ij}S^{kl}\right)^{1/2}$$

$$\frac{\mathcal{D}\sigma_e}{\mathcal{D}_t} = \frac{3}{2\sigma_e}S_j^i\frac{\mathcal{D}\tau_i^j}{\mathcal{D}t} = \frac{3}{2\sigma_e}g_{ik}g_{jl}S^{kl}\frac{\mathcal{D}\tau^{ij}}{\mathcal{D}t}$$

$$D_e^{(p)} = \left(\frac{2}{3}d_j^{i(p)}d_i^{j(p)}\right)^{1/2} = \left(\frac{2}{3}g^{ik}g^{jl}d_{ij}^{(p)}d_{kl}^{(p)}\right)^{1/2}$$

$$D_e = \left(\frac{2}{3}d_j^i d_i^j\right)^{1/2}$$

$$d_j^{i(p)} = D_j^{i(p)} - \frac{1}{3}\delta_j^i g^{kl}D_{kl}^{(p)} = D_j^{i(p)},\ d_j^i = D_j^i - \frac{1}{3}\delta_j^i g^{kl}D_{kl}$$

$$E_{te}^{(p)} = \frac{\mathcal{D}\sigma_e}{\mathcal{D}t}\Big/D_e^{(p)},\ E_{te} = \frac{\mathcal{D}\sigma_e}{\mathcal{D}t}\Big/D_e$$

$$E_{se} = \sigma_e/\epsilon_e$$

$$\epsilon_e^{(p)} = \int_0^t D_e^{(p)}\,\mathrm{d}t,\quad \epsilon_e = \int_0^t D_e\,\mathrm{d}t$$

$$\alpha = \begin{cases} 1, \text{ when } \sigma_e = \sigma_{e_{\max}} \text{ and } \dfrac{\mathcal{D}\sigma_e}{\mathcal{D}t} > 0 \text{ (plastic loading)} \\ 0, \text{ when } \sigma_e < \sigma_{e\max} \text{ or } \dfrac{\mathcal{D}\sigma_e}{\mathcal{D}t} < 0 \text{ (unloading).} \end{cases}$$

In the relations above, σ_e is the equivalent stress, ϵ_e is the equivalent strain, while $E_{te}^{(p)}$, $E_{se}^{(p)}$ are the plastic tangent and secant moduli. It should be noted that $E_{te}^{(p)}$ is the ratio of the Jaumann derivative of equivalent stress $\mathcal{D}\sigma_e/\mathcal{D}t$ and the plastic equivalent strain rate $D_e^{(p)}$, it is not equal to the slope of the plastic equivalent stress–strain curve.

Transformation between contravariant, covariant and mixed tensor components allows eqns (7) and (8) to be expressed as

$$D_{ij} = C_{ijkl}\frac{\mathcal{D}\tau^{kl}}{\mathcal{D}t} \tag{9}$$

†Essentially the same type of modification to deformation theory was used in Ref. [10].

where

$$C_{ijkl} = \frac{1}{E}\left[\frac{1+\nu}{2}(g_{ik}g_{jl} + g_{il}g_{jk}) - \nu g_{ij}g_{kl}\right] + \alpha\frac{9}{4E_{te}^{(p)}}\frac{S_{ij}S_{kl}}{\sigma_e^2}$$

in flow theory and

$$C_{ijkl} = \frac{1}{E}\left[\frac{1+\nu}{2}(g_{ik}g_{jl} + g_{il}g_{jk}) - \nu g_{ij}g_{kl}\right] + \alpha\left[\left(\frac{3}{2E_{se}} - \frac{1+\nu}{E}\right)\left(\frac{1}{2}(g_{ik}g_{jl} + g_{il}g_{jk}) - \frac{1}{3}g_{ij}g_{kl}\right) + \frac{9}{4}\left(\frac{1}{E_{te}} - \frac{1}{E_{se}}\right)\frac{S_{ij}S_{kl}}{\sigma_e}\right]$$

in modified deformation theory.
The inverse form of (9) is

$$\frac{\mathcal{D}\tau^{ij}}{\mathcal{D}t} = L^{ijkl}D_{kl} \tag{10}$$

where

$$L^{ijkl} = \frac{E}{1+\nu}\left[\frac{1}{2}(g^{ik}g^{jl} + g^{il}g^{jk}) + \frac{\nu}{1-2\nu}g^{ij}g^{kl} - \frac{3}{2\sigma_e^2}\frac{S^{ij}S^{kl}}{\left(1 + \frac{2(1+\nu)}{3E}E_{te}^{(p)}\right)}\right]$$

in flow theory and

$$L^{ijkl} = \frac{2}{3}E_{se}\left[\frac{1}{2}(g^{ik}g^{jl} + g^{il}g^{jk}) + \left(\frac{E/E_{se}}{2(1-2\nu)} - \frac{1}{3}\right)g^{ij}g^{kl} - \frac{3}{2}\left(1 - \frac{E_{te}}{E_{se}}\right)\frac{S^{ij}S^{kl}}{\sigma_e^2}\right]$$

in modified deformation theory. Both are for the case of plastic loading. During elastic deformation or unloading from a plastic state,

$$L^{ijkl} = \frac{E}{1+\nu}\left[\frac{1}{2}(g^{ik}g^{jl} + g^{il}g^{jk}) + \frac{\nu}{1-2\nu}g^{ij}g^{kl}\right].$$

The symmetric tensor of moduli L^{ijkl} is simpler in form than that (in equations (2.14) and (2.18)) of Needleman and Tvergarrd because there is no necessity for forming derivatives of the metric tensor in the up-dated Lagrangian formulation since all quantities are stated at their current value.

In the following application of the constitutive relations shown above $E_{te}^{(p)}$ is taken as E_{te} and ϵ_e is used in place of $\epsilon_e^{(p)}$ because the difference is negligibly small and it makes the computation easier.

NECKING ANALYSIS OF CYLINDRICAL BAR

In Fig. 1, a cylindrical bar with an initial axi-symmetric concave profile is shown. Both before and after deformation, the same cylindrical polar coordinates r, θ, $z(=1,2,3)$ are adopted. Non-zero velocities are

$$V_1 = \dot{U},\ V_3 = \dot{W}$$

whilst $V_2 = 0$, because of the axi-symmetric character of the problem.

The strain rates can be expressed as

$$\left.\begin{aligned} D_{11} &= \frac{\partial \dot{U}}{\partial r},\ D_{22} = \frac{\dot{U}}{r} \\ D_{33} &= \frac{\partial \dot{W}}{\partial z},\ D_{13} = \frac{1}{2}\left(\frac{\partial \dot{U}}{\partial z} + \frac{\partial \dot{W}}{\partial r}\right). \end{aligned}\right\} \tag{11}$$

The axi-symmetric version of (10) gives the constitutive relations in incremental form as

$$\left.\begin{aligned} \frac{\mathcal{D}\tau_{11}}{\mathcal{D}t} &= L_{11}D_{11} + L_{12}D_{22} + L_{13}D_{33} + 2L_{14}D_{13} \\ \frac{\mathcal{D}\tau_{22}}{\mathcal{D}t} &= L_{12}D_{11} + L_{22}D_{22} + L_{23}D_{23} + 2L_{24}D_{13} \\ \frac{\mathcal{D}\tau_{33}}{\mathcal{D}t} &= L_{13}D_{11} + L_{23}D_{22} + L_{33}D_{33} + 2L_{34}D_{13} \\ \frac{\mathcal{D}\tau_{13}}{\mathcal{D}t} &= L_{14}D_{11} + L_{24}D_{22} + L_{34}D_{33} + 2L_{44}D_{13} \end{aligned}\right\} \tag{12}$$

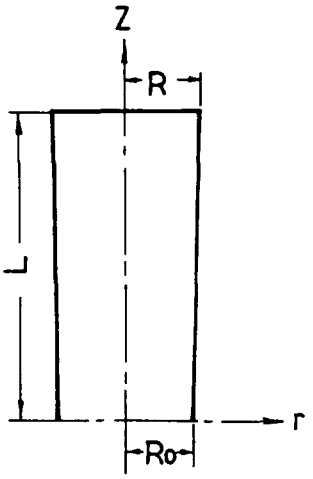

FIG. 1. An axi-symmetric specimen.

Substitution of (12) into (1) yields

$$I = \frac{1}{2}\int_0^z \int_0^r \Big\{ L_{11} D_{11}^2 + L_{22} D_{22}^2 + L_{33} D_{33}^2 + 4L_{44} D_{13}^2 + 2L_{12} D_{11} D_{22} + 2L_{13} D_{11} D_{33} + 4L_{14} D_{11} D_{13} + 2L_{23} D_{22} D_{33} + 4L_{24} D_{22} D_{13} + 4L_{34} D_{33} D_{13} - 2[\sigma_{11}(D_{11}^2 + D_{13}^2) + \sigma_{22}(D_{22}^2) + \sigma_{33}(D_{13}^2 + D_{33}^2) + 2\sigma_{13}(D_{11} + D_{33}) D_{13}] + \sigma_{11}\left[\left(\frac{\partial \dot{U}}{\partial r}\right)^2 + \left(\frac{\partial \dot{W}}{\partial r}\right)^2\right] + \sigma_{22}\left(\frac{\dot{U}}{r}\right)^2 + \sigma_{33}\left[\left(\frac{\partial \dot{U}}{\partial z}\right)^2 + \left(\frac{\partial \dot{W}}{\partial z}\right)^2\right] + 2\sigma_{13}\left(\frac{\partial \dot{U}}{\partial r}\frac{\partial \dot{U}}{\partial z} + \frac{\partial \dot{W}}{\partial r}\frac{\partial \dot{W}}{\partial z}\right)\Big\} 2\pi r \, dr \, dz. \tag{13}$$

The second integral term of (1) has disappeared from (13), since at the two ends of the bar only the displacement rate is given and there is no controlled loading rate. Boundary conditions can be expressed as

$$\left.\begin{aligned} \dot{W}(r, L, t) &= \dot{W}_0(t) \quad \text{at } z = L \\ \dot{W}(r, O, t) &= 0 \quad \text{at } z = 0 \\ \text{and } \frac{\partial \dot{U}}{\partial z}(r, z, t) &= 0 \quad \text{at } z = 0, L. \end{aligned}\right\} \tag{14}$$

The last boundary condition implies shear-free surfaces at the middle section and at both ends of the bar. For $z = 0$ it is rigorously equivalent to the shear-free condition, while at $z = L$ the final computation gives a shear stress as little as 10^{-15} of the axial stress σ_z.

For the purposes of numerical work it is convenient to normalize the physical variables in the following way.

$$\bar{I} = \frac{I}{\pi R^2 L E}, \quad \bar{z} = \frac{z}{L}, \quad \bar{r} = \frac{r}{R}, \bar{L} = \frac{L + \Delta L}{L}, \rho = \frac{L}{R}$$

$$\bar{W}_0 = \frac{\Delta L}{L}, \bar{U} = \frac{U}{R}, \bar{W} = \frac{W}{L}, \bar{E}_{te} = \frac{E_{te}}{E}, \bar{E}_{se} = \frac{E_{se}}{E}$$

$$\bar{\sigma}_{ij} = \frac{\sigma_{ij}}{E}, \bar{\tau}_{ij} = \frac{\tau_{ij}}{E}, \bar{T}_{ij} = \frac{T_{ij}}{E}, \bar{S}_{ij} = \frac{S_{ij}}{E}, \bar{L}_{ij} = \frac{L_{ij}}{E}$$

(13) and (14) now become

$$\bar{I} = \int_0^{\bar{L}} \int_0^{\bar{R}_i} \Big\{ (\bar{L}_{11} - \bar{\sigma}_{11})\left(\frac{\partial \dot{\bar{U}}}{\partial \bar{r}}\right)^2 + (\bar{L}_{22} - \bar{\sigma}_{22})\left(\frac{\dot{\bar{U}}}{\bar{r}}\right)^2 + (\bar{L}_{33} - \bar{\sigma}_{33}) \left(\frac{\partial \dot{\bar{W}}}{\partial \bar{z}}\right)^2 + \left(\bar{L}_{44} - \frac{\bar{\sigma}_{11}}{2} + \frac{\bar{\sigma}_{33}}{2}\right)\frac{1}{\rho^2}\left(\frac{\partial \dot{\bar{U}}}{\partial \bar{z}}\right)^2 + (2\bar{L}_{44} - \bar{\sigma}_{11} - \bar{\sigma}_{33})$$

$$\frac{\partial \dot{\bar{U}}}{\partial \bar{z}}\frac{\partial \dot{\bar{W}}}{\partial \bar{r}}+\left(\bar{L}_{44}+\frac{\bar{\sigma}_{11}}{2}-\frac{\bar{\sigma}_{33}}{2}\right)\rho^2\left(\frac{\partial \dot{\bar{W}}}{\partial \bar{r}}\right)^2+2\bar{L}_{12}\frac{\partial \dot{\bar{U}}}{\partial \bar{r}}\frac{\dot{\bar{U}}}{\bar{r}}+2\bar{L}_{13}\frac{\partial \dot{\bar{U}}}{\partial \bar{r}}\frac{\partial \dot{\bar{W}}}{\partial \bar{z}}$$
$$+2\bar{L}_{14}\frac{1}{\rho}\frac{\partial \dot{\bar{U}}}{\partial \bar{r}}\frac{\partial \dot{\bar{U}}}{\partial \bar{z}}+2(\bar{L}_{14}-\bar{\sigma}_{13})\rho\frac{\partial \dot{\bar{U}}}{\partial \bar{r}}\frac{\partial \dot{\bar{U}}}{\partial \bar{r}}+2\bar{L}_{23}\frac{\dot{\bar{U}}}{\bar{r}}\frac{\partial \dot{\bar{W}}}{\partial \bar{z}}+2\bar{L}_{24}\frac{1}{\rho}\frac{\bar{U}}{\bar{r}}\frac{\partial \dot{\bar{U}}}{\partial \bar{z}}$$
$$+2\bar{L}_{24}\rho\frac{\dot{\bar{U}}}{\bar{r}}\frac{\partial \dot{\bar{W}}}{\partial \bar{r}}+2(\bar{L}_{34}-\bar{\sigma}_{13})\frac{1}{\rho}\frac{\partial \dot{\bar{W}}}{\partial \bar{z}}\frac{\partial \dot{\bar{U}}}{\partial \bar{z}}+2\bar{L}_{34}\rho\frac{\partial \dot{\bar{W}}}{\partial \bar{z}}\frac{\partial \dot{\bar{W}}}{\partial \bar{r}}\Bigg\}\bar{r}\,\mathrm{d}\,\bar{r}\,\mathrm{d}\,\bar{z} \tag{15}$$

and

$$\left.\begin{aligned}&\dot{\bar{W}}=\dot{\bar{W}}_0(t) && \text{at } \bar{z}=1,\\ &\dot{\bar{W}}=0 && \text{at } \bar{z}=0,\\ &\frac{\partial \dot{\bar{U}}}{\partial \bar{z}}=0 && \text{at } \bar{z}=0,1\end{aligned}\right\} \tag{16}$$

In order to improve the accuracy of the computation, Lagrange multipliers are added to approximately satisfy the lateral side conditions of

$$\bar{\sigma}_{11}=0,\quad \bar{\sigma}_{13}=0.$$

For the sake of simplicity, the following side constraints K^i are substituted for the above conditions and are imposed on the necking part of the bar only

$$\left.\begin{aligned}&\frac{\mathscr{D}\bar{\tau}_{11}}{\mathscr{D}t}\Big|_{r=R_i}=(\bar{L}_{11}D_{11}+\bar{L}_{12}D_{22}+\bar{L}_{13}D_{33}+2\bar{L}_{14}D_{13})\Big|_{r=R_i}=0,\\ &\frac{\mathscr{D}\bar{\tau}_{13}}{\mathscr{D}t}\Big|_{r=R_i}=(\bar{L}_{14}D_{11}+\bar{L}_{24}D_{22}+\bar{L}_{34}D_{33}+2\bar{L}_{44}D_{13})\Big|_{r=R_i}=0\end{aligned}\right\} \tag{17}$$

where R_i stands for the outer radius of the bar at each discrete section plane.†

According to (5) the functional for solution is

$$\bar{I}_\lambda=\bar{I}+\lambda_i^{(1)}\frac{\mathscr{D}\bar{\tau}_{11}}{\mathscr{D}t}\Big|_{r=R_i}-\lambda_i^{(2)}\frac{\mathscr{D}\bar{\tau}_{13}}{\mathscr{D}t}\Big|_{r=R_i}. \tag{18}$$

The following relations between different stress rates or derivatives are needed in the computation

$$\left.\begin{aligned}&\dot{\bar{\tau}}_{11}=\frac{\mathscr{D}\bar{\tau}_{11}}{\mathscr{D}t}-2(\bar{\sigma}_{11}D_{11}+\bar{\sigma}_{13}D_{13}),\\ &\dot{\bar{\tau}}_{22}=\frac{\mathscr{D}\bar{\tau}_{22}}{\mathscr{D}t}-2(\bar{\sigma}_{22}D_{22}),\\ &\dot{\bar{\tau}}_{33}=\frac{\mathscr{D}\bar{\tau}_{33}}{\mathscr{D}t}-2(\bar{\sigma}_{33}D_{33}+\bar{\sigma}_{13}D_{13}),\\ &\dot{\bar{\tau}}_{13}=\frac{\mathscr{D}\bar{\tau}_{33}}{\mathscr{D}t}-(\bar{\sigma}_{11}D_{13}+\bar{\sigma}_{13}D_{33}+\bar{\sigma}_{13}D_{11}+\bar{\sigma}_{33}D_{13})\end{aligned}\right\} \tag{19}$$

and

$$\left.\begin{aligned}&\dot{\bar{T}}_{11}=\dot{\bar{\tau}}_{11}+\left(\bar{\sigma}_{11}D_{11}+\bar{\sigma}_{13}\frac{1}{\rho}\frac{\partial \dot{\bar{U}}}{\partial \bar{z}}\right),\\ &\dot{\bar{T}}_{22}=\dot{\bar{\tau}}_{22}+\bar{\sigma}_{22}D_{22}\\ &\dot{\bar{T}}_{33}=\dot{\bar{\tau}}_{33}+\left(\bar{\sigma}_{13}\rho\frac{\partial \dot{\bar{W}}}{\partial \bar{r}}+\bar{\sigma}_{33}D_{33}\right),\\ &\dot{\bar{T}}_{13}=\dot{\bar{\tau}}_{13}+\left(\bar{\sigma}_{11}\rho\frac{\partial \dot{\bar{W}}}{\partial \bar{r}}+\bar{\sigma}_{13}D_{33}\right),\\ &\dot{\bar{T}}_{31}=\dot{\bar{\tau}}_{13}+\left(\bar{\sigma}_{13}\frac{\partial \dot{\bar{U}}}{\partial \bar{r}}+\bar{\sigma}_{33}\frac{1}{\rho}\frac{\partial \dot{\bar{U}}}{\partial \bar{z}}\right).\end{aligned}\right\} \tag{20}$$

†This condition involves only the first term of (3), but it is quite satisfactory because the stresses on the boundary calculated without the side constraints are just about 2% of the maximum stress in the neck and, anyway, the first term is numerically dominant in (3).

The relations between the components of true stress and nominal stress are

$$\left.\begin{aligned}
\bar{\sigma}_{11} &= (1+D_{11})\bar{T}_{11} + \frac{1}{\rho}\frac{\partial \dot{\bar{U}}}{\partial \bar{z}}\bar{T}_{31} \\
\bar{\sigma}_{22} &= (1+D_{22})\bar{T}_{22} \\
\bar{\sigma}_{33} &= \rho\frac{\partial \dot{\bar{W}}}{\partial \bar{r}}\bar{T}_{13} + (1+D_{33})\bar{T}_{33} \\
\bar{\sigma}_{13} = \bar{\sigma}_{31} &= \rho\frac{\partial \dot{\bar{W}}}{\partial \bar{r}}\bar{T}_{11} + (1+D_{33})\bar{T}_{31} = (1+D_{11})\bar{T}_{13} \\
&\quad + \frac{1}{\rho}\frac{\partial \dot{\bar{U}}}{\partial \bar{z}}\bar{T}_{33}.
\end{aligned}\right\} \tag{21}$$

NUMERICAL COMPUTATIONS AND RESULTS

A solution is sought in the form of a three term expansion in the radial coordinate, namely

$$\left.\begin{aligned}
\dot{\bar{U}} &= U_1(\bar{z}, t)\bar{r} + U_2(\bar{z}, t)\bar{r}^3 + U_3(\bar{z}, t)\bar{r}^5, \\
\dot{\bar{W}} &= W_1(\bar{z}, t) + W_2(\bar{z}, t)\bar{r}^2 + W_3(\bar{z}, t)\bar{r}^4.
\end{aligned}\right\} \tag{22}$$

The functions U_j and W_j $(j = 1, 2, 3)$ are held, at each value of the generalized time t, by their values $(U_j)_i$ and $(W_j)_i$ at the ith axial section of the bar; the n sections of the bar are taken to be all equal in length. Along the radial direction of each section plane, m nodes are recorded for numerical integration. The computation within each increment Δt of time proceeds as follows.

(a) Specify the value of the increment $\Delta \bar{W}_0$ of the normalized axial displacement at the end of the bar. In the present computations $\bar{W}_0$ is taken to be the generalized time t.

(b) At each nodal point the plastic moduli to be used in the current load step are computed from the assumed relation between equivalent stress and strain and the values of these quantities at the end of the previous load step. In particular, the inverse $1/\bar{E}_{t\epsilon}$ of the tangent modulus is read from a table similar to Table 1 as a function of ϵ_e, whilst the normalized secant modulus at each node point is taken as

$$\bar{E}_{s\epsilon} = \frac{\bar{\sigma}_e}{\epsilon_e}.$$

If the material is unloading or elastic, the moduli are the elastic ones.

(c) The functional $\bar{I}_\lambda$ of (18) can now be evaluated using the trapezoidal rule for the integrations and a three-point finite-difference formula for the axial derivatives. The variational relationships

$$\frac{\partial \bar{I}_\lambda}{\partial (U_j)_i} = 0, \quad \frac{\partial \bar{I}_\lambda}{\partial (W_j)_i} = 0$$

subject to the discretized version of the boundary conditions (16), allow a matrix equation for the unknowns to be formulated, and the inversion produces a solution of the form

$$\left.\begin{aligned}
(U_j)_i &= (a_{ij})_i \Delta \bar{W}_0 + [(a_{2j})_i]_k \lambda_k^{(1)} + [(a_{3j})_i]_k \lambda_k^{(2)}, \\
(W_j)_i &= (b_{ij})_i \Delta \bar{W}_0 + [(b_{2j})_i]_k \lambda_k^{(1)} + [(b_{3j})_i]_k \lambda_k^{(2)}
\end{aligned}\right\} \tag{23}$$

in terms of the known displacement increment and the, as yet, unknown Lagrange multipliers. The summation variable k ranges from 1 to l where l is the number of plane sections on which the side conditions (17) are forced.

(d) The substitution of (23) into the side conditions (17) produces a system of equations that can be inverted to give the $\lambda_i^{(1)}$ and $\lambda_i^{(2)}$ in terms of $\Delta \bar{W}_0$. These values may then be fed back into (23) and (22) to complete the solution for the field of velocity.

Table 1. $\epsilon_e - (1/\bar{E}_{t\epsilon})$ $E = 207$ GPa, $\nu = 0.29$

ϵ_e	0.010	0.030	0.040	0.050	0.065	0.080
$1/\bar{E}_{te}$	68	76	90	120	142	154
ϵ_e	0.100	0.120	0.140	0.500	0.800	1.100
$1/\bar{E}_{te}$	236	340	440	450	460	470

(e) The Jaumann derivative of Kirchhoff stress $\mathcal{D}\tau_{ij}/\mathcal{D}t$ may now be calculated from (11) and (12), then the Jaumann derivative of equivalent stress is

$$\frac{\mathcal{D}\bar{\sigma}_e}{\mathcal{D}t} = \frac{3}{2\bar{\sigma}_e}\left(\bar{S}_{11}\frac{\mathcal{D}\bar{\tau}_{11}}{\mathcal{D}t} + \bar{S}_{22}\frac{\mathcal{D}\bar{\tau}_{22}}{\mathcal{D}t} + \bar{S}_{33}\frac{\mathcal{D}\bar{\tau}_{33}}{\mathcal{D}t} + 2\bar{S}_{13}\frac{\mathcal{D}\bar{\tau}_{13}}{\mathcal{D}t}\right)$$

and, finally, the convected derivative of nominal stress may be found from (19) and (20).

(f) During the increment Δt the nominal stress changes to

$$\bar{T}_{ij} = \bar{T}_{ij} + \dot{\bar{T}}_{ij}\Delta t.$$

The new values of true stress $\bar{\sigma}_{ij}$ are calculated from (21), taking into account the change of area at each node.

(g) At each point the equivalent stress and strain are computed.

(h) New equal axial sections are set up and new radial integration nodes introduced. The values of the stress and plastic moduli are interpolated onto the new node points, and the process (a)–(h) is repeated for the next increment of time.

The total time of the simulation is divided into about five or six sections. At the end of each section, the computed load are compared with those of the experiment[1] under simulation. If there is any significant disagreement, the relation between the total equivalent strain and the tangent moduli is adjusted, the data in Table 1 are renewed, and the results are re-computed. This process is repeated until the agreement is reached. A check is made with the experimentally measured thinning at the neck.

This computational method was used to study the necking of a cylindrical bar with an initial axi-symmetric concave profile. Both flow theory and modified deformation theory were used as the plastic constitutive model. Experimental data[1] for specimen 2499R was simulated in the computation. The material was specified as A-533 Grade B Class 1 nuclear pressure vessel steel[1]. The half length of the specimen was 26.67 mm, with maximum radius 6.41 mm and minimum radius 6.35 mm. The current normalized length $\bar{L}$ was divided into 24 equal parts with 11 nodes along the radial direction of each section. Starting from $z = 0$, 10 sections were subjected to the side constraints in (17).

The computed simulation of the equivalent stress–strain curve is shown in Fig. 2 (in which the difference between total strain and plastic strain is neglected). Unloading during necking takes place after $\epsilon_e \doteq 0.1$. The results of Fig. 2 can alternatively be expressed in terms of the inverse values of the normalized tangent modulus, and these are listed in Table 1. Linear interpolation is used for determining $\bar{E}_{ie}$ from this table.

The complete computation takes a little more than 300 steps of increment Δt (i.e. $\Delta \bar{W}_0$), which is made to vary with the total elongation $\bar{W}_0$ according to the data of Table 2. The convergence of the solution was checked by halving the increment of time. The whole computation then took about 600 steps to attain $\bar{W}_0 = 0.25$. The values of stress, necking radius and unloading area, obtained in the two computer runs, are shown in Table 3 and it is seen that the solution has effectively converged in 300 steps.

The maximum magnitude of the calculated radial stress and shear stress at the lateral boundary in the necking region is about 10^{-4} of the axial stress and 10^{-3} of the radial stress on the axis. This occurs when the elongation $\bar{W}_0 = 0.25$, just before fracture happens. Before that stage, the values of the lateral boundary

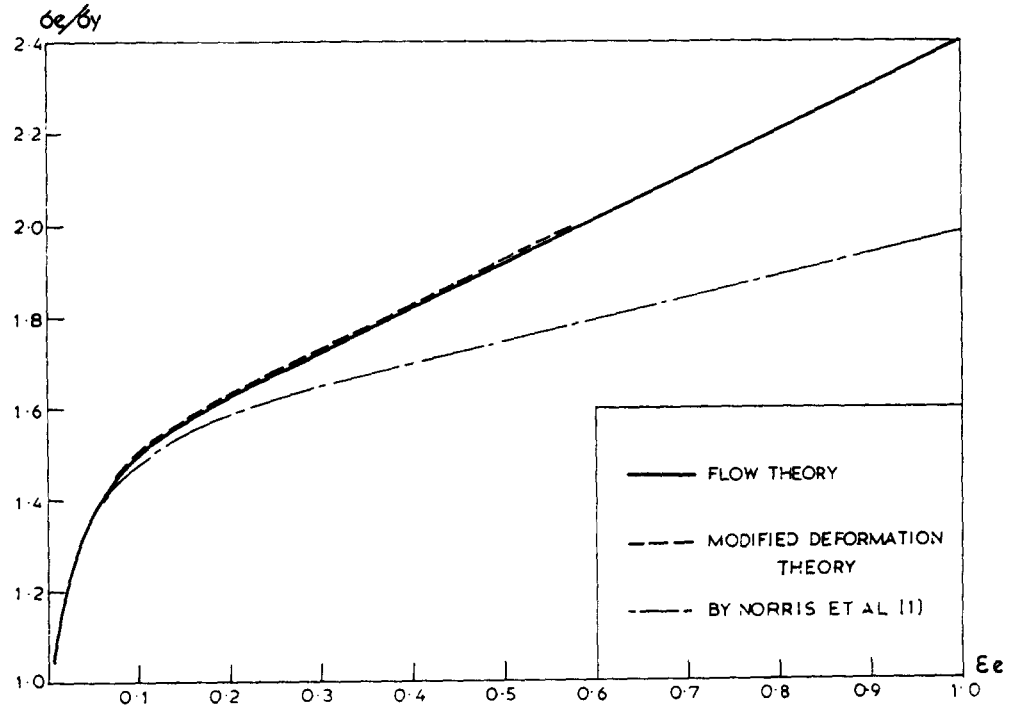

FIG. 2. Computer simulation curve of equivalent stress vs equivalent strain.

Table 2. $\bar{W}_0 - \Delta\bar{W}_0$

$\bar{W}_0\ (10^{-2})$	$\Delta\bar{W}_0\ (10^{-5})$
0.22 - 0.35	1 - 50
0.35 - 4.3	200
4.3 - 10	150
10 - 20	75
>20	50

radial and shear stresses are much smaller. It is concluded that the lateral free surface conditions are correctly represented in the computations.

Fig. 3 shows the relationship between the normalized current minimum radius r_0/R and the normalized axial elongation $\Delta L/L$. Fig. 4 shows the variation of axial load ratio F/F_{max} with $\Delta L/L$. At different stages of necking, the border lines between the domains of plastic loading and unloading are obtained by using each of the two plasticity theory and can be seen in Fig. 5. From the trend shown in these figures it may be concluded that, with the same value of tangent modulus E_t, the thinning of the neck calculated according to modified deformation theory is larger than that according to flow theory. Also, the unloading rate of the former is larger than that of the latter. However, when $\Delta L/L$ exceeds 0.16, the predictions of deformation theory depart from the experimentally observed thinning and the only way agreement could be matched would be to adjust Table 1 appropriately. Therefore, the computation based on modified deformation theory was terminated when $\Delta L/L$ reached 0.18. The results thus obtained are then compared with those based on flow theory using the same value of tangent modulus.

The distribution of stress according to flow theory is shown in Fig. 6. The computed results demonstrate that just before the specimen fractures the axial stress tends to zero within a small domain near $\bar{z} = 0.36$. This is similar to that shown in Fig. 10 of [1], where it is stated that a small region is stressed by axial compression. A careful examination of Fig. 6 also shows that the hoop stress $\bar{\sigma}_\theta$ in the neck reduces as necking develops. This is the same tendency as that shown in Fig. 8 of [1]. On the other hand, Saje[3] states that this surface compression component decreases and may even become tensile.

The results of different workers[1–4] over the last decade are compared with the present computations in Fig. 7. All the stress distributions are rather smooth. The present computations were also carried out

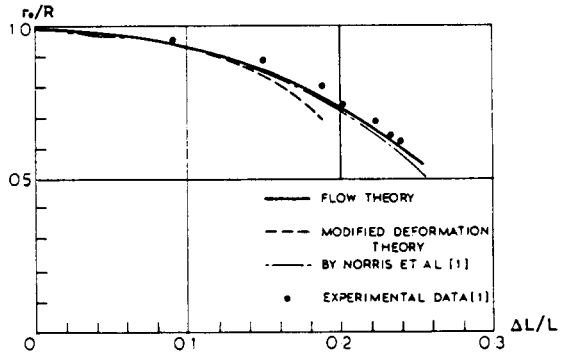

FIG. 3. Relationship between the normalized current minimum radius with the normalized axial elongation.

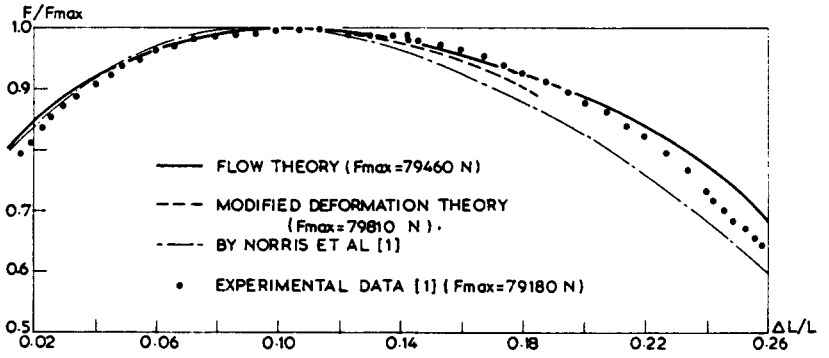

FIG. 4. Variation of axial load ratio with normalized axial elongation.

Table 3.

$\bar{W}_0$	load steps	$\bar{\sigma}_{33max}(10^{-2})$	r_0/R	unloading border
0.140	300	0.398	0.878	same
	600	0.395	0.879	
0.186	300	0.491	0.776	same
	600	0.487	0.777	
0.250	300	0.755	0.566	same
	600	0.750	0.568	

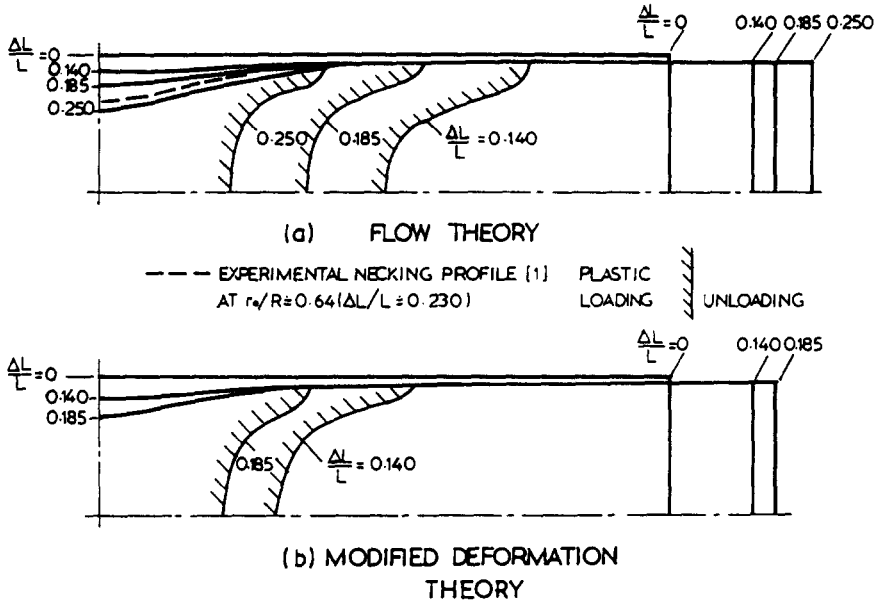

FIG. 5. Border line between plastic loading and unloading domains.

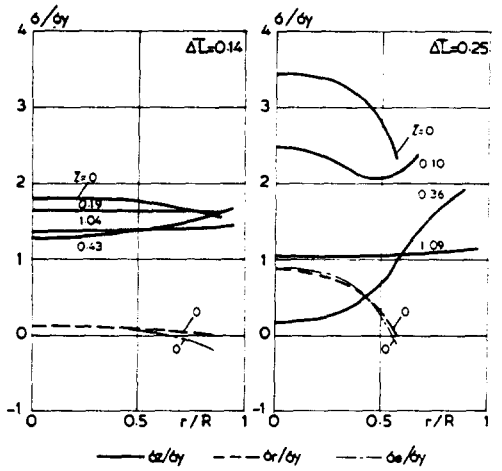

FIG. 6. Stress distributions at different stages of necking.

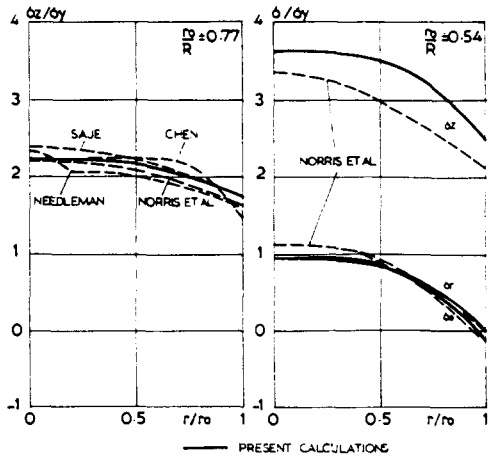

FIG. 7. Comparison of stress distributions by present analysis with those of other references (at $\bar{z} = 0$).

without using the Lagrange multipliers, with a saving of about one third of the computer time, but with somewhat of a loss of accuracy. The lateral boundary radial stress in the neck could attain about 2% of the maximum axial stress, instead of the order of 10^{-4} when Lagrange multipliers were used, at $\bar{W}_0 = 0.25$. At the same time, the peak axial stress shifted from the central axis. Saje[3] also mentions the peak of stress distribution moved away when coarser finite-difference grids were used.

The equivalent stress shown in Fig. 2 is somehat higher than that obtained by Norris *et al.*[1], although the same computer simulation was used. It appears that this is due to the present computations being closer to most of the experimental data. Both Fig. 3 and Fig. 4 show that the results of Norris *et al.* fall away from the experimental data after necking happens (at $\epsilon_e = 0.1$). This is the point where the present simulated equivalent stress–strain curve diverges from that of Norris *et al.*

CONCLUSIONS

It may be concluded that both flow theory and modified deformation theory may serve to simulate necking. With the same relationship between the tangent modulus and equivalent strain these two theories give practically the same result before necking occurs, whilst after necking the latter theory yields a larger necking deformation with a larger unloading rate. From the good agreement obtained between the calculated results and the existing experimental data, it seems that the one-dimensional discretization using up-dated Lagrangian description is an appropriate method for computation. The values of the normal strain and the stresses at the centre of the bar, generated by simulation studies, are needed in any attempt to unravel the details of ductile fracture. The present simulated stress–strain curve and other aspects of this work are being used in computations of ductile void growth.

Acknowledgement—Many thanks are due to Dr. I. C. Howard for his kindly help and discussion in presenting this paper.

REFERENCES

1. D. M. NORRIS, JR., B. MORAN, J. K. SCUDDER and D. F. QUINONES, A computer simulation of the tension test. *J. Mech. Phys. Solids* **26**, 1 (1978).
2. W. H. CHEN, Necking of a bar. *Int. J. Solids Structures* **7**, 685 (1971).
3. MIRAN SAJE, Necking of a cylindrical bar in tension. *Int. J. Solids Structures* **15**, 731 (1979).
4. A. NEEDLEMAN, A numerical study of necking in circular cylindrical bar. *J. Mech. Phys. Solids* **20**, 111 (1972).
5. R. HILL, Eigenmodal deformations in elastic/plastic continua. *J. Mech. Phys. Solids* **15**, 371 (1967).
6. R. M. MCMEEKING and J. R. RICE, Finite-element formulations for problems of large elastic–plastic deformation. *Int. J. Solids Structures* **11**, 601 (1975).
7. B. BUDIANSKY, A reassessment of deformation theories of plasticity. *J. Appl. Mech.* **26**, 259 (1959).
8. J. CHRISTOFFERSEN and J. W. HUTCHINSON, A class of phenomenological corner theories of plasticity. *J. Mech. Phys. Solids* **27**, 465 (1979).
9. A. NEEDLEMAN and V. TVERGARRD, Necking of biaxially stretched elastic–plastic circular plates. *J. Mech. Phys. Solids* **25**, 159 (1977).
10. R. ABEYARATNE and N. TRIANTAFYLLIDIS, The emergence of shear bands in plane strain. *Int. J. Solids Structures* **17**, 1113 (1981).